Available online at www.HEFJournal.org

ISSN: 2785-2997

Journal of
Human, Earth, and Future

Vol. 7, No. 2, June, 2026

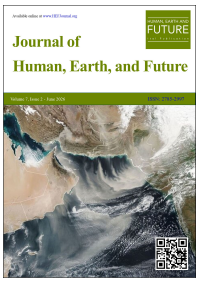

Autonomous UV-C Robotic Disinfection for CT Suites: Efficacy, Safety, and Protocol Development

Sanchai Eardprab [1], Bhuvaneswari Kandasamy [2], Marut Tangwattanachuleeporn [3], Alisara Wongsuttilert [4], Taweelarp Tansavatdi [4], Sarun Phibanchon [5], Surachai Wongcharee [6], Pravech Ajawatanawong [7], Kowit Suwannahong [8*]

[1] *Faculty of Engineering, Burapha University, Chonburi 20131, Thailand.*

[2] *Department of Physics, Faculty of Science and Humanities, SRM University Delhi-NCR, Sonepat, Haryana 131029, India.*

[3] *Faculty of Allied Health Sciences, Burapha University, Chonburi 20131, Thailand.*

[4] *Faculty of Medicine, Burapha University, Chonburi 20131, Thailand.*

[5] *Department of Innovation and Educational Technology, Burapha University, Chonburi 20131, Thailand.*

[6] *Field of Environmental Engineering, Faculty of Engineering, Mahasarakham University, Mahasarakham 44150, Thailand.*

[7] *Department of Microbiology, Faculty of Medicine Siriraj Hospital, Mahidol University, Bangkok 10700, Thailand.*

[8] *Faculty of Public Health, Burapha University, Chonburi 20131, Thailand.*

Received 31 December 2025; Revised 28 April 2026; Accepted 04 May 2026; Published 01 June 2026

Abstract

This study developed and evaluated an autonomous UV-C robotic disinfection system for computed tomography (CT) examination rooms, assessing microbial inactivation efficacy and operational safety using bacterial and viral surrogates. *Staphylococcus aureus* ATCC 25923 and bacteriophage were used as surrogates. The UV-C robot, equipped with eight low-pressure mercury lamps (36 W, 254 nm), was tested in two phases: localized irradiation at exposure times of 2-8 minutes and whole-room disinfection across five critical surfaces during a 21-minute operational cycle. Residual ozone concentrations were continuously monitored throughout all trials. The UV-C robot achieved complete inactivation of bacteriophages within 4 minutes and a greater than 99.99% reduction (>4 log) in *Staphylococcus aureus* colony counts at the same exposure time. Ozone concentrations remained consistently below occupational exposure limits (maximum 0.0043 ppm vs. OSHA limit of 0.1 ppm) throughout all trials. This study provides the first comprehensive evaluation of autonomous UV-C robotic disinfection specifically designed for CT suite geometries, integrating both efficacy testing and real-time safety monitoring. The findings establish evidence-based protocols for implementing UV-C robotic disinfection in diagnostic imaging departments and support the clinical feasibility of such systems as adjuncts to standard infection control practices.

Keywords: Autonomous UV-C Disinfection Robot; Pathogen Contamination; High-Touch Surfaces; SARS-CoV-2; Clinical Environments; Medical Devices; Mathematical Modeling.

1. Introduction

Coronavirus disease 2019 (COVID-19) has transitioned from an acute global health emergency to an endemic respiratory infection that requires sustainable, long-term management strategies. While emerging variants continue

* Corresponding author: kowit.su@go.buu.ac.th

https://doi.org/10.28991/HEF-2026-07-02-08

to warrant surveillance, current epidemiological evidence indicates no substantial increase in disease severity compared to previously circulating strains [1–4]. Nevertheless, regional resurgences persist, with Thailand documenting over 53,000 new cases between 18–24 May 2025, predominantly affecting adults aged 20–39 years and demonstrating sustained community transmission [5]. These trends underscore the continued importance of robust infection control measures, particularly in healthcare settings where vulnerable populations are concentrated [6–9].

Computed tomography (CT) systems constitute an integral component of modern diagnostic imaging, providing high-resolution cross-sectional visualization for trauma assessment, oncological staging, vascular evaluation, and pulmonary diagnosis [10]. During the COVID-19 pandemic, CT imaging proved instrumental in assessing pulmonary involvement and monitoring disease progression. However, the shared, high-throughput nature of CT suites presents inherent infection control challenges due to frequent patient turnover, close staff-patient interaction, and repeated contact with high-touch surfaces, including gantries, control consoles, and positioning accessories [11–13]. Experimental evidence has demonstrated that severe acute respiratory syndrome coronavirus 2 (SARS-CoV-2) remains viable for extended periods on commonly encountered materials—up to 72 hours on plastic, 48 hours on stainless steel, 24 hours on cardboard, and 4 hours on copper, highlighting the potential for fomite-mediated transmission in inadequately decontaminated environments [14].

Surface decontamination strategies for SARS-CoV-2 inactivation encompass chemical and physical modalities [15, 16]. Although chemical disinfectants remain widely used, their effectiveness is constrained by variability in application, human error, material incompatibility, and incomplete surface coverage. Consequently, complementary physical disinfection technologies capable of delivering consistent, reproducible antimicrobial performance have garnered increasing attention [17].

Ultraviolet germicidal irradiation (UVGI), specifically within the UV-C spectrum (200–280 nm), represents an established physical disinfection modality for healthcare environments [18–20]. UV-C radiation induces photochemical damage to microbial nucleic acids, generating pyrimidine dimers that prevent DNA replication and render pathogens non-infectious [21, 22]. Wavelengths approximating 254 nm demonstrate high efficacy against diverse microorganisms, including methicillin-resistant *Staphylococcus aureus* (MRSA), *Clostridioides difficile*, and viral pathogens such as Ebola virus and influenza [23, 24]. Recent investigations have confirmed that SARS-CoV-2 is highly susceptible to UV-C radiation, with complete viral inactivation achieved within minutes at sufficient doses [25]. Low-pressure mercury lamps emitting primarily at 254 nm remain among the most widely used and regulatory-approved UVGI sources due to their stable output, demonstrated efficacy, and compatibility with existing infrastructure [26].

The integration of UV-C technology into autonomous robotic platforms represents a significant advancement in healthcare disinfection. Many studies focus on laboratory-scale experiments or static room disinfection scenarios [27, 28]. There is limited evaluation in real-world clinical environments, such as CT rooms. Mehta et al. [18] comprehensively reviewed UV disinfection robots, highlighting their potential for consistent, contactless decontamination while reducing reliance on manual processes. Anderson et al. [29] demonstrated that enhanced terminal room disinfection incorporating UV-C technology significantly reduced healthcare-associated infections caused by multidrug-resistant organisms. Similarly, Boyce & Donskey [24] emphasized the role of automated “no-touch” disinfection technologies in supplementing conventional cleaning protocols to address incomplete manual decontamination.

Despite the documented germicidal efficacy of UV-C radiation, several critical gaps persist in the current literature. First, most studies focus on laboratory-scale experiments or static-room disinfection, with limited evaluation in real-world clinical environments with complex equipment geometries, such as CT suites [30, 31]. Second, few investigations systematically integrate assessments of disinfection efficacy with comprehensive operator safety evaluations, particularly real-time monitoring of UV-C irradiance and ozone by-products parameters crucial for clinical implementation yet frequently underreported [32]. Third, insufficient validation using appropriate viral surrogates representative of respiratory pathogens limits the extrapolation of findings to clinically relevant scenarios [33]. Fourth, standardized protocols for UV-C robot deployment in diagnostic imaging departments remain absent, hindering reproducible implementation across healthcare facilities [34].

In response to these identified gaps, the present study systematically evaluates the efficacy and safety of an autonomous UV-C disinfection robot designed specifically for CT suite environments. The system incorporates eight 36-W low-pressure mercury lamps emitting germicidal radiation at 254 nm, providing a rapid, chemical-free alternative to conventional manual disinfection. The study objectives were fourfold: (I) to quantify time-dependent microbial reduction using standardized bacterial (*Staphylococcus aureus* ATCC 25923) and viral (bacteriophage)

surrogates across exposure durations of 2, 4, 6, and 8 minutes; (II) to evaluate whole-instrument disinfection performance across five high-touch CT surfaces in a comprehensive operational cycle; (III) to conduct real-time safety monitoring of UV-C irradiance and ambient ozone concentrations throughout operation; and (IV) to develop mathematical models characterizing relationships among exposure duration, UV-C intensity, ozone generation, and microbial reduction efficiency. By integrating rigorous efficacy assessment with comprehensive safety monitoring and appropriate surrogate validation, this study addresses critical gaps in the UVGI literature and provides evidence supporting the clinical feasibility of autonomous UV-C disinfection technologies in high-throughput diagnostic imaging environments.

2. Materials and Methods

2.1. Materials

The autonomous UV-C disinfection system comprised eight low-pressure mercury lamps (Philips TUV 36W SLV/6), generating germicidal irradiation at 254 nm. Omnidirectional locomotion was achieved through a Mecanum wheel configuration, with navigation autonomy enabled by an Arduino Mega 2560 microcontroller interfaced with infrared proximity detectors and ambient light sensors. Independent power supplies were allocated for locomotion and germicidal subsystems to ensure operational reliability. Irradiance measurements were obtained using a calibrated UV-C radiometer (Lutron UVC-254 SD), while ambient ozone levels were monitored via a photometric analyzer (Model 400E).

Laboratory instrumentation encompassed steam sterilization equipment (HICLAVE HVE-50, Hirayama, Japan), bacterial incubation system (Contherm Polar 1000c, New Zealand), sample homogenizer (S0200, Thermo Fisher Scientific, USA), dry-heat sterilization oven (BINDER-ED 56, Germany), precision micropipette (Eppendorf G18315G, Germany), refrigerated storage unit (RT 300W, Hitachi, Japan), and optical densitometer (DEN-1, Labnet International, Latvia). Culture media (nutrient agar; HiMedia, India) and sterile consumables, including sampling swabs (SOFTIP, Longmed, Thailand), Petri dishes (90 × 15 mm; Corning, France), and borosilicate culture tubes (16 × 150 mm; PYREX, Mexico), were utilized throughout the investigation. The direct extrapolation of surrogate inactivation data to SARS-CoV-2 requires caution, given structural differences, though enveloped viruses typically exhibit greater UV-C susceptibility than non-enveloped bacteriophages. Laboratory-controlled conditions may not fully replicate the complex bioburden encountered in active clinical environments.

2.2. Detailed Design of the Experiment

The experimental framework for evaluating the autonomous UV-C disinfection robot is illustrated in Figure 1. Disinfection efficacy was assessed against *S. aureus* (ATCC 25923) and bacteriophage MS2 as bacterial and viral challenge organisms, respectively. Surrogate selection adhered to international surface disinfection standards (EN 13697; ASTM E2197) and EPA/WHO guidance for coronaviral surrogates based on documented UV-C inactivation characteristics analogous to SARS-CoV-2 [4, 31]. All procedures were conducted within a computed tomography suite (470 × 640 × 300 cm) under controlled environmental conditions (temperature: 20-22°C; relative humidity: 68-72%). Microbiological manipulations were performed aseptically in a Class II biological safety cabinet in accordance with established biosafety guidelines (CDC & NIH, 2020) under Institutional Biosafety Committee authorization (Protocol 021/2564).

The experimental design comprised two phases. Phase I (Reduction on a Single Surface) examined microbial reduction on a single surface irradiated from a 1-meter distance across exposure durations of 2, 4, 6, and 8 minutes. Test surfaces were inoculated with standardized microbial suspensions, air-dried under ambient conditions, and subsequently exposed to UV-C irradiation at predetermined intervals. Phase II (Whole-instrument Disinfection) evaluated disinfection performance across five high-touch CT surfaces, namely: (1) CT couch, (2) front of CT gantry, (3) back of CT gantry, (4) CT console, and (5) CT scan surface. Mathematical modeling was performed to investigate: (I) average irradiation versus time, (II) UV-C intensity versus time, (III) O_3 release versus UV-C intensity, and (IV) linear correlation between average number of colonies versus UV-C disinfection efficiency.

Microbial recovery was conducted using sterile swabs, followed by cultivation on nutrient agar at 37°C for 24-48 hours prior to colony enumeration. While the selected surrogates provide internationally validated efficacy data, direct extrapolation to SARS-CoV-2 warrants appropriate caution due to viral envelope structural differences; however, enveloped viruses typically demonstrate greater UV-C susceptibility than non-enveloped bacteriophages, suggesting that the present findings represent conservative efficacy estimates.

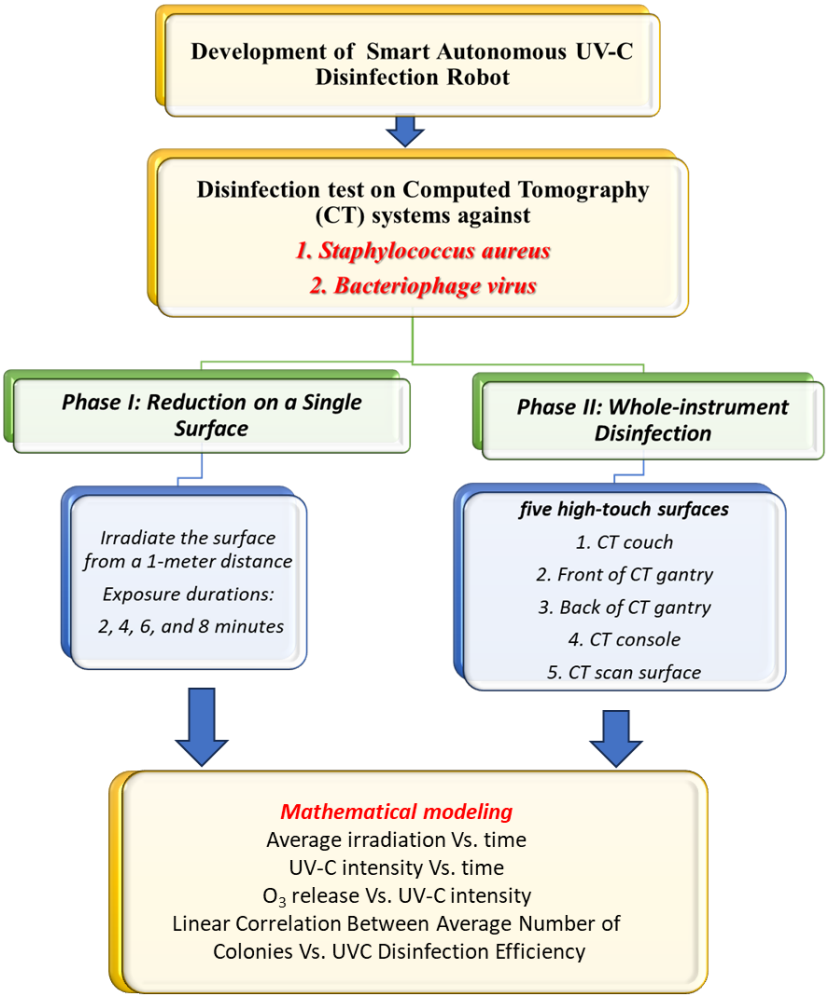

Figure 1. Flowchart illustrating the detailed experimental design

2.3. Development and Functionality of UV-C Disinfection Robot

The robot has a compact structure with a square base measuring 35 cm on each side and a total height of 110 cm. It is equipped with eight low-pressure mercury UV-C lamps (Philips TUV 36W SLV/6), each emitting 36 watts of UV-C light at a wavelength of 254 nm (Figure 2).

Figure 2. (a) The UV-C disinfection smart autonomous robot and (b) during working

Robot Structure and Components

The automated UV-C disinfection robot is a compact, self-navigating device designed to reduce pathogen contamination on high-touch surfaces in clinical settings, particularly in CT scanner rooms. Measuring 35 × 35 × 110 cm, the robot is engineered for effective disinfection and agile maneuverability in confined spaces.

The robot consists of two primary components:

- UV-C Disinfection Unit: This unit features eight low-pressure mercury UV-C lamps (Phillips TUV 36W SLV/6), each emitting germicidal light at 254 nanometers. The lamps are mounted vertically, with two on each of the robot's four sides, maximizing exposure to surrounding surfaces and enhancing disinfection coverage. The electronic control system and dedicated battery pack are housed below the lamp assembly, ensuring proper weight distribution and shielding sensitive components from direct UV-C radiation. The robot features a red housing that encloses a high-performance inverter, which converts battery-supplied direct current (DC) into alternating current (AC) to power the UV-C lamps. This configuration maintains consistent, stable light output during use.
- Mobility System and Control Mechanisms: The robot features four Mecanum wheels for omnidirectional movement, controlled by an Arduino Mega 2560 microcontroller. It uses five infrared (IR) line-tracking sensors to autonomously follow black tape on the floor. When all five sensors detect a cross line, the robot stops and activates the UV-C lamps for a preset disinfection period. Once complete, it resumes movement. For operational flexibility, the system can also be controlled remotely. The mobility and lamp systems are powered by separate batteries, ensuring the UV-C output remains stable regardless of mobility demands.

This robot's design emphasizes practicality, flexibility, and cost-effectiveness. Affordable, straightforward IR sensors eliminate the need for complex navigation systems, such as LiDAR or SLAM. Replacing floor tape enables quick route adjustments, making it ideal for dynamic healthcare environments. Developed during the COVID-19 pandemic, the robot provides a reliable, efficient solution for rapid hospital deployment, ensuring effective microbial disinfection with minimal setup and resource requirements.

2.4. *S. aureus* Preparations

Stimulate *S. aureus* by cross-streaking on Nutrient agar (Himedia, India) and incubating at 37 °C. Suspend the *S. aureus* colony in 0.85% standard saline solution (NSS) for 18 hours, then adjust the turbidity to match a 0.5 McFarland standard using a densitometer. Use the prepared suspension within 15 minutes. The microbial load was confirmed by the spread plate technique following a 10-fold serial dilution. *S. aureus* (ATCC 25923) was selected as the standard test organism for surface disinfection efficacy testing per EN 13697 and ASTM E2197 protocols. Its higher UV-C resistance compared with most Gram-negative bacteria provides conservative estimates of efficacy, and its clinical relevance as a pathogen commonly associated with healthcare-acquired infections makes it an appropriate bacterial indicator.

2.5. Host Preparation for Bacteriophage Virus

To prepare the Host B-2 culture for bacteriophage quantification, first grow the culture at 37°C for 24 hours. After incubation, scrape the Host B-2 colony and transfer it into Nutrient Broth (NB) medium. Dilute the suspension 10-fold. Next, aspirate 0.5 mL of the Host B-2 suspension at the desired dilution (in this case, 10^6) from the tube and transfer it to a new test tube for further use. The bacteriophage was selected as a surrogate for enveloped RNA viruses, as recommended by the EPA and the WHO for studies of disinfection efficacy. The non-pathogenic nature of bacteriophages allows safe laboratory handling at the high titers required for disinfection validation. Previous studies have demonstrated comparable UV-C susceptibility between bacteriophages and coronaviruses, making this surrogate appropriate for evaluating disinfection systems against respiratory pathogens. While these surrogates provide valuable efficacy data validated against international standards, direct extrapolation to SARS-CoV-2 inactivation should be interpreted with appropriate caution, as viral envelope structure, surface stability, and environmental persistence may differ between the surrogate and the target organism.

2.6. Bacteriophage Virus Plaque Quantification

To quantify the concentration of a bacteriophage, begin by diluting the virus stock using the 10-fold dilution method until reaching a final dilution of 10^{-6}. Then, mix 0.5 mL of the diluted virus solution with 0.5 mL of Host B-2 suspension in a test tube and incubate at 37°C for 10 minutes. After incubation, transfer the entire 1 mL solution onto a Nutrient Agar (NA) plate and gently spread it across the surface. Incubate the plate at 37°C for 10 minutes to allow plaque formation. Finally, calculate the viral concentration by counting plaques and applying the formula to determine the plaque-forming units per milliliter (PFU/mL):

$$\text{Plaque} - \text{Forming Units} = \frac{\text{Number of Plaques}}{\text{Dilution factor} * \text{Volume of Plated}} \quad (1)$$

2.7. UV-C Disinfection Unit and Irradiance Measurement

UV-C irradiance measurements were conducted using a calibrated UVC radiometer (Lutron UVC-254 SD) positioned at predetermined locations throughout the CT suite to characterize spatial dose distribution. The radiometer was oriented perpendicular (90°) to the lamp surface at a standardized distance of one meter from the lamp center. The autonomous robot was programmed to navigate through five strategic stopping positions designed to maximize angular coverage around the CT gantry, ensuring comprehensive UV-C exposure of all target surfaces. Irradiance readings were recorded at two-minute intervals throughout the disinfection cycle to quantify the cumulative UV-C dose delivered to environmental surfaces.

The UV-C dose (D, in μJ/cm^2) was determined using the formula:

$$D = I \times t \tag{2}$$

where, I represents irradiance in mW/cm^2 and t denotes exposure time in minutes.

The UV-C light intensity was measured to be approximately 0.143 mW/cm^2 at a distance of 1 m. When applied appropriately, this intensity was sufficient to inactivate various microorganisms and viruses, including SARS-CoV-2.

2.8. Ozone Measurement

Ozone production was monitored during the UV-C irradiation process to assess safety levels. A photometric ozone analyzer (model 400E) was used to measure ozone concentrations before, during, and after the UV-C irradiation cycle. Ozone levels were recorded at 1-minute intervals, and the peak concentration was noted to ensure it remained below hazardous levels [35].

2.9. Statistical Analysis

Sample size (n = 3 independent replicates per experimental condition) was determined a priori based on preliminary pilot data and biosafety laboratory capacity constraints, providing sufficient statistical power to detect biologically meaningful differences (>1 $\log_{10}$ reduction) between treatment conditions. Microbial reduction efficacy was quantified as $\log_{10}$ reduction values for each surface type and irradiation duration. Data normality was verified using the Shapiro-Wilk test ($p > 0.05$ for all datasets), and homogeneity of variances between groups was confirmed by Levene's test ($p > 0.05$), satisfying the assumptions for parametric analysis. Comparisons of microbial counts before and after UV-C treatment were performed using Student's t-test, with statistical significance set at $\alpha = 0.05$. Effect sizes were calculated using Cohen's d to evaluate the practical significance of observed reductions, with $d > 0.8$ indicating large effects. Results are expressed as mean ± standard deviation (SD), with 95% confidence intervals (CI) reported for primary outcome measures [36].

2.10. UV-C Inactivation Mechanisms

UV-C radiation (wavelength 200-280 nm) inactivates microorganisms through photochemical damage to nucleic acids. At the optimal germicidal wavelength of 254 nm, UV photons are absorbed by the aromatic bases of DNA and RNA, leading to the formation of pyrimidine dimers (primarily thymine-thymine and cytosine-cytosine dimers). These dimers distort the DNA helix structure, blocking DNA replication and transcription, thereby rendering the microorganism non-infectious.

The dose-response relationship follows first-order inactivation kinetics described by the Chick-Watson model:

$$N/N_0 = e^{-kD} \tag{3}$$

where, N_0 is the initial microbial count, N is the surviving count after UV exposure, k is the rate constant (organism-specific UV susceptibility), and D is the UV dose (mJ/cm²). This model predicts that the surviving microbial fraction (N/N_0) decreases exponentially with increasing UV dose, while the log reduction ($\log_{10} N_0/N$) increases linearly with dose, a prediction validated by our experimental observations.

2.11. Mobility and Autonomous Operation

The UV-C disinfection robot is designed to operate autonomously with remote control capabilities. It moves along a predefined path in the CT room (Figure 3), using a tracking system embedded in its mobility platform. A remote sensing tool and a light sensor, positioned 1 cm above the robot's body, guide its navigation. The disinfection begins with activating the UV-C lamps, followed by the robot's movement along its designated path. Upon reaching the endpoint, the robot automatically halts both its movement and irradiation, ensuring precise and controlled disinfection.

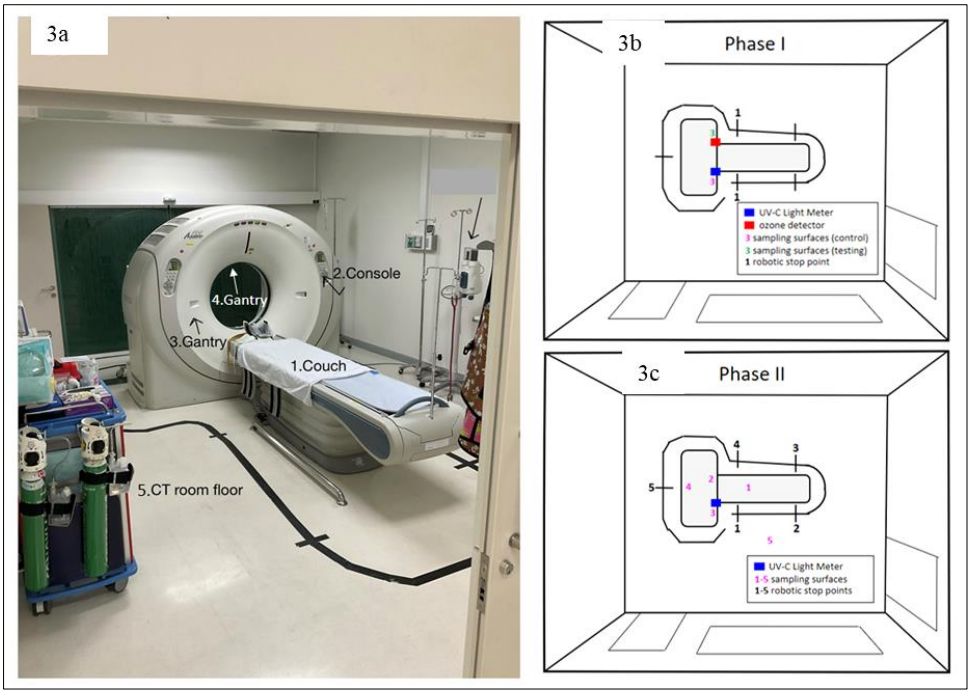

Figure 3. Experimental setup. (a) Layout of the CT room; (b) Phase I: Control surface (pink) and test surface (green) on the CT console, with UV-C light meter (blue) and ozone detector (red) placed at the test surfaces. Robot irradiation at 1 m distance for 2, 4, 6, and 8 minutes; (c) Phase II: Five sampling surfaces with five robotic stop points, each irradiated for 4 minutes, and UV-C light meter (blue) at CT console surface (3) for intensity measurements.

Phase I: Microbial Reduction on a Single Surface

In phase I of the experiment, microbial reduction efficacy of the disinfection robot was evaluated on a single high-touch surface, the CT console. Before irradiation, 0.1 mL of microbial suspension containing *S. aureus* (ATCC 25923) at a concentration of 1.5 × 10^8 CFU/mL and a bacteriophage virus at 10^{-6} pfu/mL was inoculated onto the surface. A sterile cotton swab was applied to the suspension to a 9 cm x 9 cm area (81 cm^2) of the surface. After inoculation, the robot was activated and irradiated the surface from a distance of 1 meter for 2, 4, 6, and 8 minutes, and microbial reduction was assessed post-irradiation. During UV-C irradiation, the robot's low-pressure mercury (LPM) lamps emitted 254 nm UV-C radiation, which also generated 185 nm radiation and ozone. To ensure safety, ozone levels were continuously monitored using a photometric ozone analyzer (model 400E), with the maximum peak ozone concentration recorded at 0.0043 ppm after 8 minutes of irradiation.

The surface swabs were collected before and after UV-C irradiation, and pathogen reduction was assessed by plating the samples onto Nutrient Agar for bacterial colony counting and performing plaque assays for bacteriophage virus. The $\log_{10}$ reductions in microbial counts were calculated by comparing the pre- and post-irradiation samples, providing a measure of the efficacy of the UV-C smart robot in reducing microbial contamination on the CT console. All tests were carried out in triplicate to ensure statistical reliability.

Phase II: Whole-instrument Disinfection

In Phase II, the UV-C robot's efficacy in disinfecting five high-touch surfaces within the CT scan equipment was evaluated. These surfaces included the CT couch, front and back surfaces of the CT gantry, CT console, and the CT scan surface. Each surface was inoculated with the same microbial suspensions used in Phase I (*S. aureus* and bacteriophage virus). The robot followed a pre-programmed path, making five stops to irradiate each surface for 4 minutes, resulting in a total disinfection time of 21 minutes. After irradiation, microbial reduction was assessed by collecting surface samples using the same method as in Phase I. The decrease in microbial counts for each surface was calculated, and the robot's overall performance was evaluated.

Following the findings from Phase I, a four-minute duration was selected as the optimal irradiation time. The experiment took place inside a CT scan room measuring 470 cm in width, 640 cm in length, and 300 cm in height, with a total volume of 90 m^3. Environmental conditions were controlled, maintaining a temperature between 20 and 22°C and humidity levels of 68 to 72%. The CT scanner height was 100.5 cm. During the trial, the robot followed its predetermined route, irradiating each surface for 4 minutes at 1 meter, for a total of 21 minutes of exposure. All procedures were conducted without personnel present to ensure safety from UV-C exposure.

3. Results and Discussion

Table S1 presents the irradiance and UV-C intensity values recorded by the UV-C robot at different irradiation durations of 2, 4, 6, and 8 minutes. The data show an increase in irradiance values as the exposure time progresses, with the highest value of 0.196 mW/cm^2 achieved at the 8-minute mark. This indicates that the UV-C robot generates a greater energy output over more extended irradiation periods. Similarly, the UV-C intensity, representing the cumulative energy delivered to the target surface, also rises with time, ranging from 280 μJ/cm^2 at 2 minutes to 1,544 μJ/cm^2 at 8 minutes. At 2 minutes, the UV-C intensity is relatively low. However, it is still sufficient to produce significant microbial reduction, as demonstrated in the results for both *S. aureus* and the bacteriophage virus. Increasing the exposure time to 4 and 6 minutes increases the intensity, leading to more effective microbial inactivation. By the 8-minute exposure, the peak UV-C intensity of 1,544 μJ/cm^2 corresponds to the complete eradication of bacterial and viral pathogens, highlighting the efficiency of longer irradiation durations.

3.1. Phase I Experiments

In this study, the log10 reductions of and bacteriophage viruses after exposure to UV-C light for varying durations (2, 4, 6, and 8 minutes) were calculated to assess the effectiveness of disinfection (Table S2). Before UV-C exposure, *S. aureus* colony-forming unit ranged from 2.63×10^{11} CFU/mL to 2.13×10^{11} CFU/mL, and the bacteriophage virus concentrations ranged from 1.32×10^{9} PFU/mL to 1.60×10^{9} PFU/mL. These starting concentrations ensured a high microbial load, providing a stringent test of the UV-C disinfection system's efficacy. After 4 minutes of UV-C irradiation, the bacteriophage viruses were eradicated, demonstrating the strong virucidal properties of UV-C light (Figure 4). UV-C radiation damages the nucleic acids of viruses, inhibiting their ability to replicate and ultimately inactivating them. The total eradication of bacteriophage viruses after just 4 minutes of exposure highlights the potential of UV-C as an effective disinfectant for viral pathogens.

Similarly, the bacterial colonies of *S. aureus* were too few to count (TFTC) after 4 minutes of UV-C irradiation, indicating a significant decrease in bacterial count (Figure 4). A TFTC result typically corresponds to a $\log_{10}$ reduction of at least 4, which is widely regarded as an adequate level of disinfection, particularly in environments like healthcare settings where minimizing microbial contamination is crucial.

3.2. Mechanism of Ozone Formation During UV-C Disinfection

During UV-C disinfection, short-wavelength UV (typically at 254 nm or below) interacts with atmospheric oxygen, resulting in the photochemical formation of ozone (O_3). In this study, UV-C irradiation in the range of 280 to 1,544 μJ/cm^2 was applied for surface and full-room disinfection. Although primarily intended for microbial inactivation, UV-C photons with wavelengths below 240 nm also initiate ozone generation through the following mechanism:

1. Photodissociation of Molecular Oxygen

UV-C light (particularly at wavelengths below 240 nm) provides sufficient energy to break the O=O double bond in molecular oxygen (O_2), producing two reactive atomic oxygen radicals (O):

$$O_2+h\nu\ (\lambda<240\ \text{nm}) \rightarrow 2O \quad (4)$$

2. Ozone Formation via Radical Recombination

The atomic oxygen (O) then rapidly reacts with another molecule of O_2 to form ozone (O_3):

$$O+O_2\rightarrow O_3 \quad (5)$$

3. Steady-State Ozone Concentration

Ozone concentration is influenced by UV intensity, exposure time, air composition, and ventilation. In this study, although UV-C exposure produced ozone, the measured concentrations stayed within safe limits, indicating that ozone generation was both controlled and temporary. This aligns with the applied UV-C dose range (280–1,544 μJ/cm^2), which is effective for disinfection while minimizing overproduction of ozone.

4. Ozone Decay and Safe Re-Entry

Ozone is a reactive species that naturally decomposes into O_2 over time or can be removed through ventilation systems. The brief exposure time and the full-room disinfection cycle of 21 minutes likely allowed for adequate decay before re-entering the room, preserving safe environmental conditions for human occupancy.

The limited yet effective ozone production during UV-C disinfection contributes to microbial inactivation as a secondary mechanism, complementing the direct UV-induced damage to DNA and RNA. The ozone formation observed in this study was well-regulated, with levels staying within safe exposure limits, ensuring both effective disinfection and occupational safety.

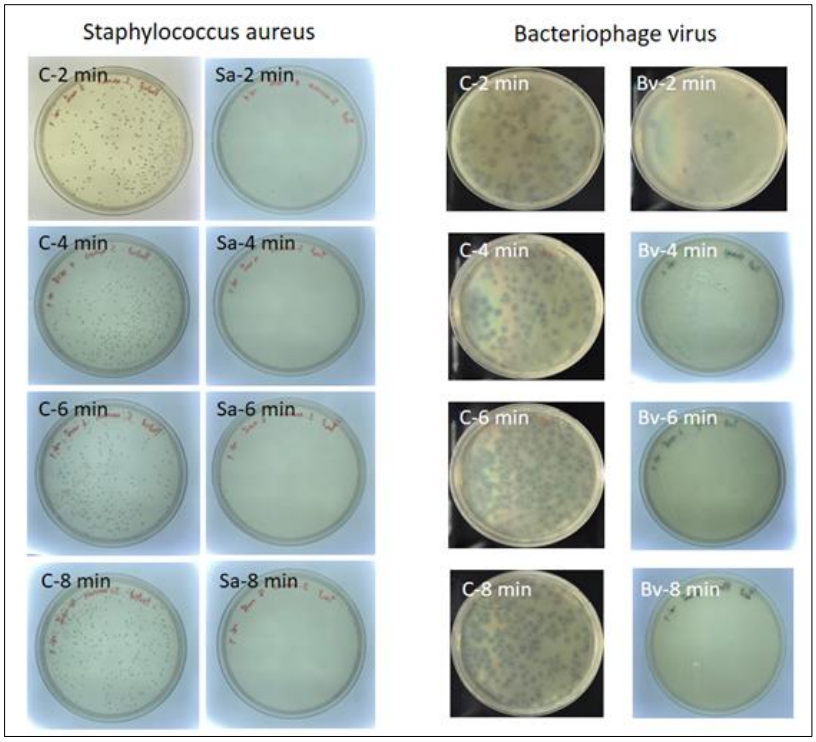

Figure 4. Biological assessment of samples collected during Phase I. Acronyms denote Control (C), *Staphylococcus aureus (Sa),* and *bacteriophage virus (Bv).*

3.3. Phase II Experiments

Phase II of the study aimed to assess the effectiveness of the autonomous UV-C disinfection robot in sanitizing various high-touch surfaces inside a CT scan room. The robot's compact design facilitated the strategic placement of quartz glass UV-C lamps (emitting at 185-254 nm), enabling optimized delivery of UV-C doses across various target surfaces. As illustrated in Figure 5, a 981 μJ/cm^2 dose was achieved on the CT console surface at 87 cm, representing the robot's capacity to maintain effective irradiance even at moderate ranges.

The robot's high mobility and precision navigation system enabled comprehensive coverage of the entire 90 m^3 CT scan room, including challenging-to-reach locations such as the corners and edges of equipment. Over a continuous 21-minute operation, the robot provided consistent disinfection, outperforming stationary systems that typically suffer from limited directional range and shadowing effects.

Representative high-contact surfaces were inoculated with *S. aureus* and *bacteriophage* suspensions to assess the microbial inactivation efficacy. The initial microbial loads ranged from approximately 5.00×10^{11} to 6.24×10^{11} CFU/mL for *S. aureus* and 3.54×10^{9} to 4.37×10^{9} PFU/mL for bacteriophages. Following a 4-minute UV-C exposure, complete inactivation of both bacterial and viral surrogates was achieved across all sampled locations (Figure 5). Notably, the CT couch irradiated at 70 cm, the gantry surfaces at 87 cm (front) and 130 cm (back), and the floor at 102 cm, each receiving adequate doses, resulting in total microbial eradication (Figure 5).

These results highlight the robot's capability to uniformly disinfect varied surfaces within a clinical imaging environment, reinforcing the advantage of autonomous UV-C systems in achieving spatial and operational efficiency. Notably, the robot's automated nature eliminates the need for manual intervention, reducing the risk of human error, cross-contamination, and occupational exposure to UV-C radiation.

The rapid and complete inactivation of both *S. aureus* and bacteriophage viruses within a 4-minute exposure period underscores the robustness of this UV-C disinfection system. These findings demonstrate the potential of the UV-C robot as a reliable infection control tool, particularly in high-risk healthcare settings where effective surface decontamination is crucial for preventing nosocomial infections. Integrating such autonomous systems into routine infection prevention protocols could substantially enhance environmental hygiene and patient safety.

Table S3 presents the results of UV-C disinfection effectiveness in removing microbial contamination from different high-touch areas of CT scan equipment. The UV-C irradiation, applied at different distances, successfully eradicated both *S. aureus* and bacteriophage virus across all tested surfaces. For instance, irradiated at a distance of 70 cm with a UV-C intensity of 981 μJ/cm^2, the CT couch resulted in the complete elimination of both pathogens. Similarly, the front

surface of the CT gantry, exposed to UV-C at 87 cm, achieved total microbial inactivation, with no detectable presence of *S. aureus* or the virus. Irradiated at 70 cm, the CT console also demonstrated total microbial eradication. The back surface of the CT gantry, irradiated from a distance of 130 cm, exhibited a significant reduction in microbial levels, with complete inactivation of both pathogens. Lastly, the CT room floor, treated with UV-C at a distance of 102 cm, achieved total disinfection. These findings highlight the efficiency of the UV-C robot in rapidly reducing microbial contamination on high-touch surfaces, underscoring its potential as an effective infection control measure in healthcare environments where swift and thorough disinfection is crucial.

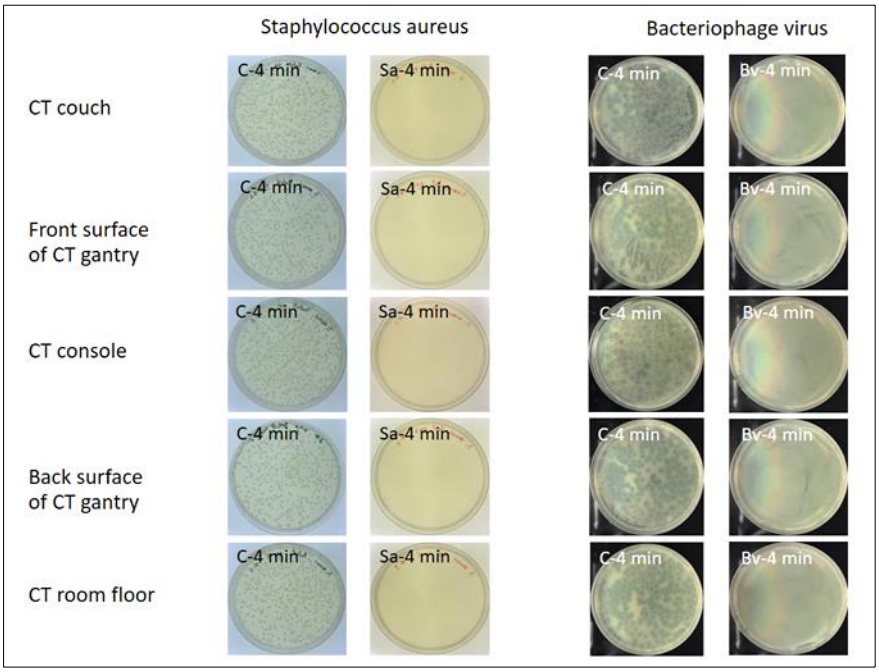

Figure 5. Schematic representation of the sampled surface areas during Phase II. Acronyms denote Control (C), *Staphylococcus aureus* (Sa), and *bacteriophage virus* (Bv).

Moreover, these findings indicate that the UV-C disinfection robot can effectively reduce the microbial load by delivering targeted irradiation to specific high-touch surfaces, thereby minimizing the risk of nosocomial infections (Figure 6). The rapid microbial inactivation observed here underscores the feasibility of implementing such systems in healthcare environments to ensure cleaner, safer surfaces and support enhanced infection control protocols.

Furthermore, the comparative analysis between Phase I and Phase II highlights the effectiveness of the UV-C disinfection robot in reducing microbial contamination across multiple surfaces in a clinical environment. While Phase I demonstrated the robot's ability to disinfect a single high-touch surface, Phase II underscored its versatility in addressing a broader range of surfaces in a healthcare setting. The 4-minute irradiation time proved effective for microbial eradication in both phases, while Phase II's 21-minute cycle time demonstrated the robot's rapid and thorough disinfection capacity. Given its proven efficacy, safety, and efficiency, the UV-C disinfection robot shows excellent promise as a tool for enhancing infection control measures in healthcare settings, offering a reliable solution for reducing the risk of healthcare-associated infections.

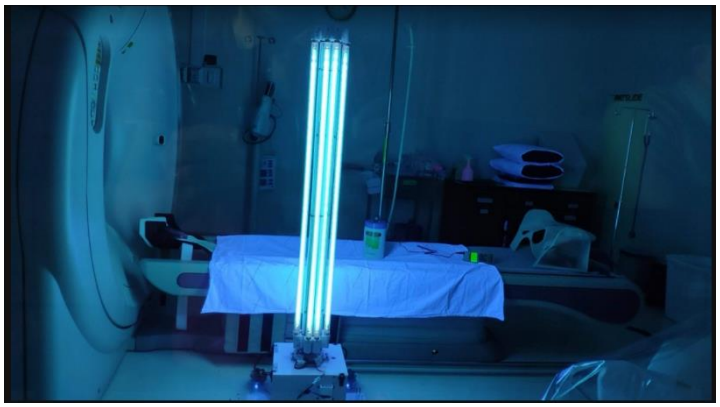

Figure 6. As developed UV-C disinfection robot

3.4. Mathematical Modeling

Assessing the UV irradiance dose and conducting relevant modeling are necessary steps to determine the performance of the developed robotic system. Hence mathematical modeling was performed to investigate in detail.

The number of colonies (n) is equal to the volume plated (v) multiplied by the dilution factor (D), and then multiplied by the colony-forming units per milliliter (CFU/ml). Figure 7(a) presents the correlation between the average number of colonies and microbial concentration following UVC exposure, evaluated for both *S. aureus* and *Bacteriophage virus*. A strong linear relationship is observed between the colony count and CFU/mL for *S. aureus*, with an R^2 value of 1.0000, indicating a highly consistent and predictable trend. This result suggests that surface colony enumeration can serve as a highly accurate indicator of bacterial viability post-irradiation. Figure 7(b) illustrates the corresponding relationship for the *Bacteriophage virus*, showing a strong, though slightly less precise, linear correlation (R^2 = 0.9281) between colony count and PFU/mL. The observed variation may reflect the inherent complexity of viral plaque formation or increased sensitivity of viruses to environmental and procedural factors. Despite this, the overall trend supports using average colony counts as a valid proxy for viral quantification in UVC disinfection assays.

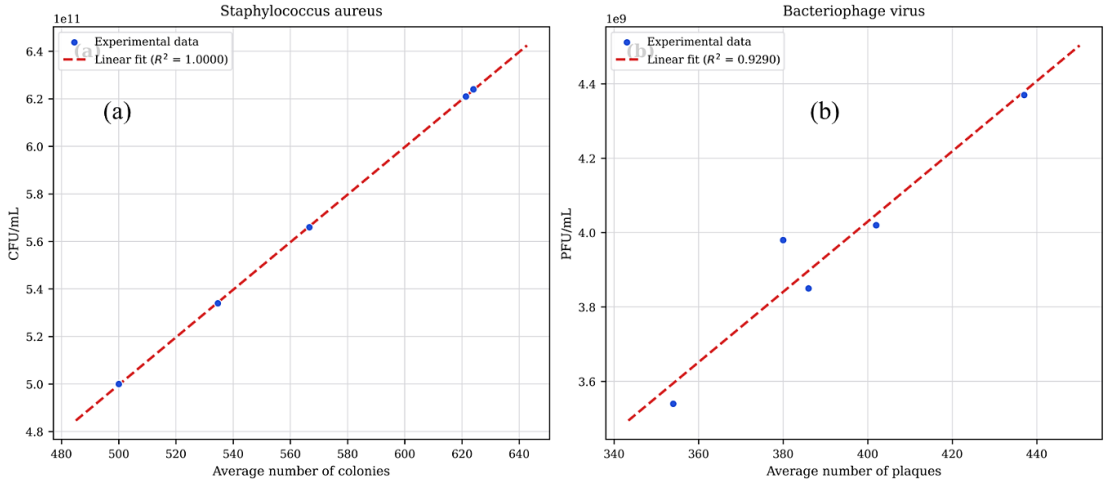

Figure 7. Linear Correlation Between Average Number of Colonies and Measured CFU/mL and PFU/mL for Evaluating UVC Disinfection Efficiency Against (a) *S. aureus*, and (b) Bacteriophage Virus

Figure 8(a) shows that the robot's average irradiance increased with increasing exposure duration. Initially, the values were low (~0.14 mW/cm^2) and rose to approximately 0.19 mW/cm^2 by the 8-minute mark. The most rapid increase occurred between the 4- and 6-minute intervals, suggesting a non-linear relationship. This trend is likely due to the stabilization of UV-C lamp output over time and improved exposure geometry as the robot moved. The mathematical model, which included a temporal factor representing lamp warm-up and surface-coverage efficiency, effectively captured the rising pattern.

Irradiance often increases as the lamp warms up and becomes more efficient. A commonly used form is an exponential saturation model or a quadratic polynomial:

$$E(t)=E_{max}(1-e^{-kt}) \quad (6)$$

where, E(t) is irradiance at time t, E_{max} is the maximum attainable irradiance, k is the irradiance constant (depends on lamp type and system configuration), and t is the time (minutes).

For the linear-to-quadratic trend,

$$E(t)=at^2+bt+c \quad (7)$$

where, a, b, and c are empirically determined coefficients.

Figure 8(b) shows a similar upward trend in UV-C intensity, increasing from about 0.0023 mW/cm^2 to 0.0032 mW/cm^2 across the same period. Because the robot maintained a consistent distance from the target surfaces, these variations can be primarily attributed to the lamp's output characteristics rather than spatial changes. The model described this intensity increase using a time-sensitive function reflecting the lamp's stabilization behavior. This approach enabled the prediction of realistic intensity profiles under prolonged operation.

UV-C intensity could be modeled similarly, especially if it's proportional to irradiance. A linear growth or exponential model can be applied:

$$I(t)=I_0+mt \quad or \quad I(t)=I_{max}(1-e^{*-t}) \quad (8)$$

where, I(t) is the intensity at time t, I_0 is the initial intensity, m is the linear growth rate, and k is the time constant. The temporal dynamics of UV-C irradiance and intensity and their influence on ozone (O_3) production were analyzed using empirical data collected from a UV-C disinfection robot operating at preset intervals of 2, 4, 6, and 8 minutes. These observations were used to evaluate and support the predictive performance of a time-dependent mathematical model developed for this purpose. The relation between UV-C intensity and ozone release is highlighted in Figure 8(c). Here, ozone concentration increased almost linearly with increasing UV-C intensity, ranging from approximately 0.0027 ppm at lower intensities to over 0.0042 ppm at the highest measured values. This outcome supports the model's assumption that ozone formation is driven by the photolysis of molecular oxygen under UV-C exposure. The nearly linear trend indicates that ozone generation is proportional to intensity within the tested range. However, minor deviations at higher levels suggest the onset of secondary effects such as ozone decomposition or reaction with environmental constituents. Figure 8(d) presents a fitted logarithmic relationship between ozone (O_3) concentration and UV-C light intensity. Experimental data indicate that O_3 release increases with increasing UV-C intensity, but at a progressively slower rate. This trend is well described by a logarithmic function of the form:

$$[O_3] = a \cdot \ln(I) + b \tag{9}$$

where, $[O_3]$ is the measured ozone level (ppm), ln(I) is the UV-C intensity (μW/cm²), and a and b are constants derived from curve fitting.

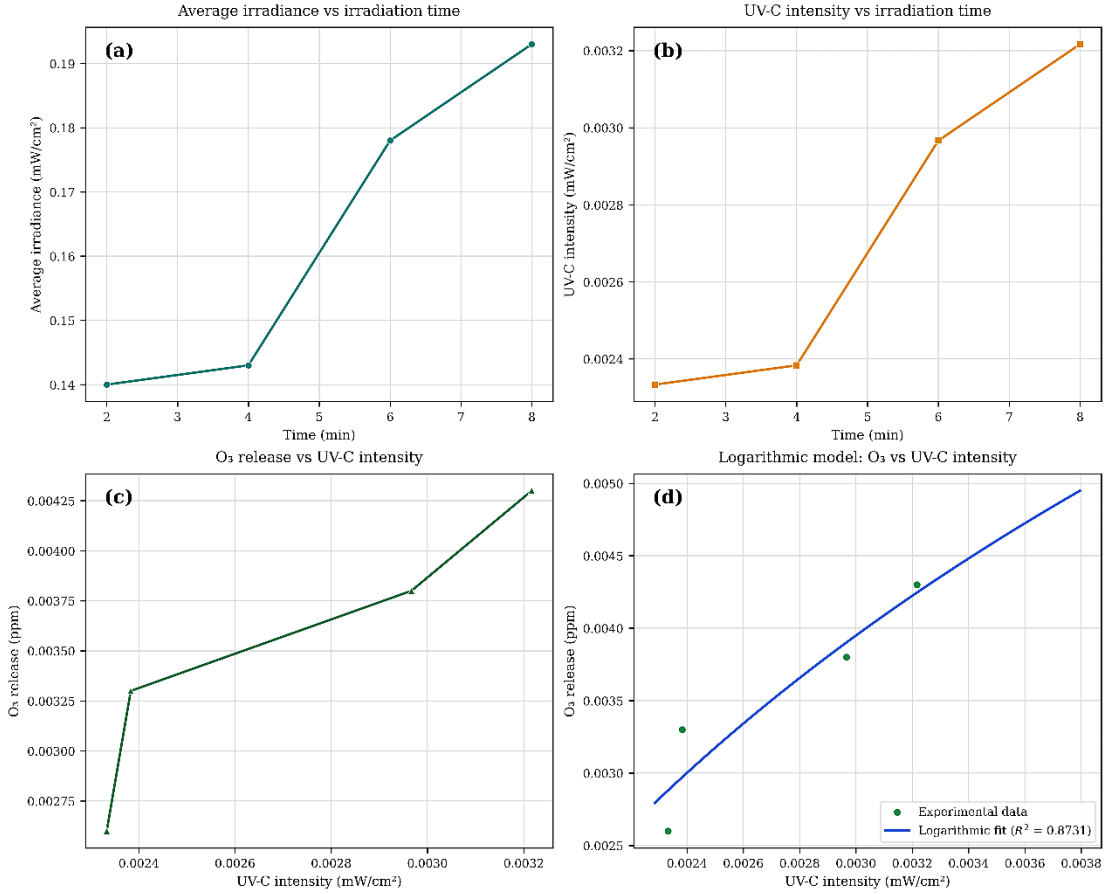

Figure 8 (a) average irradiance as a function of irradiation time, (b) UV-C intensity vs. Irradiation time, (c) ozone release as a function of UV-C intensity, and (d) logarithmic fit: O_3 concentration vs. UV-C intensity

The model exhibits a strong statistical fit, with an R^2 value of 0.8731, indicating that the logarithmic expression effectively captures the relationship between UV-C exposure and ozone generation. This suggests that while ozone production rises with increasing intensity, the rate of increase begins to taper off, a behavior that aligns with physical expectations [37, 38].

Initially, higher UV-C intensity leads to more efficient photo dissociation of oxygen molecules, thereby producing more ozone. However, ozone formation slows at higher intensities, likely due to photodecomposition or a reaction plateau driven by environmental saturation. The results collectively validate the mathematical model's structure and assumptions, demonstrating its ability to effectively simulate disinfection-relevant parameters and safety-critical by-products. It is a practical tool for determining optimal exposure times to maximize UV-C effectiveness while minimizing ozone accumulation. This is particularly relevant in enclosed or clinical environments, where safe air

quality is essential during and after robotic disinfection. The observed correlation between increased exposure time and higher UV-C intensity underscores the importance of optimizing irradiation duration to achieve maximum disinfection.

The disinfection performance of the autonomous UV-C robot is summarized in Table 1. During Phase I (single surface evaluation), UV-C doses ranging from 280 to 1,544 μJ/cm^2 were delivered, corresponding to exposure durations of 1 to 5 minutes. A clear dose-response relationship was observed, with microbial inactivation increasing in a proportional manner with UV-C exposure. At 4-minute exposure (1,235 μJ/cm^2), mean $\log_{10}$ reduction for *S. aureus* exceeded 4 $\log_{10}$ (complete inactivation in all replicates; $p < 0.001$ vs. untreated controls; Cohen's $d > 0.8$). Bacteriophage MS2 was completely inactivated after 4-minute exposure across all replicates ($p < 0.001$ vs. controls). Extended exposure to 5 minutes (1,544 μJ/cm^2) achieved near-total elimination of all test microorganisms (>5 $\log_{10}$ reduction).

Table 1. Comparative Analysis of UV-C Disinfection Robot Performance

Parameter	Exposure Time (min)	UV-C Dose (μJ/cm^2)	*S. aureus* Log Reduction	Bacteriophage Inactivation	Ozone Level (ppm)
Single Surface (Phase I)	2	17,160	Moderate (1–2 log)	Partial	0.0012
	4	34,320	Significant (>4 log)	Complete	0.0024
	6	51,480	Near-complete (>4 log)	Complete	0.0036
	8	68,640	Complete (>5 log)	Complete	0.0043
Multi-surface (Phase II)	4(×5 surfaces) = 21 mins	34,320/surface	Consistently high	Complete	< 0.0043

Phase II evaluated multi-surface disinfection under simulated clinical conditions. Five high-touch surfaces within a computed tomography (CT) suite were irradiated sequentially for 4 minutes each. Consistent disinfection efficacy (>4 $\log_{10}$ reduction) was maintained across all surface types, including stainless steel, plastic composite, and glass interfaces. Ambient ozone concentrations remained below 0.0043 ppm throughout all treatment cycles, representing less than 10% of the most stringent occupational exposure limit (ACGIH TLV and WHO guideline: 0.05 ppm) and less than 5% of OSHA and NIOSH permissible limits (0.1 ppm), as detailed in Table 2.

Table 2. Comparison of ambient ozone concentrations during UV-C robot operation with international occupational exposure limits

Regulatory Body	Exposure Limit	Averaging Time
OSHA PEL	0.1 ppm	8-hour TWA
NIOSH REL	0.1 ppm	Ceiling
ACGIH TLV	0.05 ppm (light work)	8-hour TWA
WHO Guidelines	0.05 ppm	8-hour average
Present Study (max)	0.0043 ppm	Peak during operation

Table 3. Comparison of UV-C disinfection system efficacy against microbial indicators

Study	UV-C System	Target Organism	Log Reduction	Exposure Time
Present study	Autonomous robot (8×36W)	*S. aureus*, Bacteriophage	>4 log	4 min
Astrid et al. (2021) [36]	UV-C robot	Mixed flora	2-3 log	Variable
Casini et al. (2019) [19]	UV-C LED device	*S. aureus*, *E. coli*	3-4 log	10 min
Różańska et al. (2023) [39]	UV-C radiation	MRSA, C. difficile	3-5 log	10 min

As shown in Table 3, the autonomous UV-C disinfection robot developed in this study demonstrated remarkable germicidal performance, achieving a greater than 4 log reduction against both *S. aureus* and bacteriophage MS2 within only 4 minutes of exposure. This performance substantially exceeds that of previously reported UV-C systems, which typically require 10 minutes or more to achieve comparable or lower microbial inactivation levels. Astrid et al. [36] reported only 2-3 log reductions with a UV-C robot against mixed flora, whereas Casini et al. [19] and Różańska et al. [39] achieved 3-5 log reductions but required 10-minute exposure times. The superior efficacy of our system is attributable to the optimized configuration of eight 36W UV-C lamps, which ensures a uniform, high-intensity irradiance distribution across target surfaces. Furthermore, autonomous navigation enables strategic positioning to maximize germicidal coverage, thereby addressing the shadowing limitations inherent in stationary UV-C devices. The combination of rapid disinfection cycle time and high log reduction makes this system particularly suitable for healthcare settings where minimizing room turnaround time is critical for operational efficiency and infection prevention.

Experimental microbial challenge concentrations were set substantially above documented environmental bioburden in healthcare settings to provide a rigorous assessment of germicidal efficacy (D4). The bacterial (*S. aureus*: 10^{10}-10^{11} CFU/mL) and viral surrogate (bacteriophage: 10^{8}-10^{9} PFU/mL) inocula employed in this study represent approximately 2-4 $\log_{10}$ higher concentrations than those reported in clinical environmental surveillance studies [32-34]. The demonstrated >4 $\log_{10}$ reduction achieved within a 4-minute exposure cycle under these elevated challenge conditions confirms that the autonomous UV-C system possesses sufficient germicidal capacity to effectively inactivate pathogens at contamination levels encountered in routine healthcare operations.

Table 4. Comparison of experimental microbial challenge levels and real-world healthcare surface contamination

Parameter	Experimental Level	Real-World CT Suite	Source
Surface contamination	1.5×10^{9} CFU/mL inoculum	2.5×10^{3} CFU/100cm^2 mean	Palmqvist et al. (2019) [40]
S. aureus concentration	10^{10}-10^{11} CFU/mL	10^{2}-10^{4} CFU/100cm^2	Huslage et al. (2010) [41]
Viral load	10^{8}-10^{9} PFU/mL	10^{2}-10^{5} copies/mL	Zhou et al. (2020) [42]

4. Conclusion

This study successfully developed and validated an autonomous UV-C robotic disinfection system specifically designed for computed tomography (CT) examination rooms. The key findings demonstrate that the robot achieved highly effective microbial inactivation, with complete eradication of bacteriophage virus within 4 minutes and greater than 99.99% (>4 log) reduction in *Staphylococcus aureus* under optimized operating conditions. These results confirm the system's ability to eliminate both bacterial and viral pathogens representative of healthcare-associated infections, including surrogate organisms used in respiratory pathogen studies. The safety assessment revealed that residual ozone concentrations remained consistently below established occupational exposure limits across all experimental trials (maximum recorded: 0.0043 ppm, compared with the OSHA permissible exposure limit of 0.1 ppm and the ACGIH TLV of 0.05 ppm), confirming the system's suitability for deployment in clinical healthcare facilities. The IR line-tracking navigation system demonstrated reliable autonomous operation within the complex CT suite geometry, achieving consistent coverage of predetermined disinfection positions across the 21-minute operational cycle.

From a practical perspective, this study provides evidence-based protocols for UV-C robotic disinfection in diagnostic imaging departments. The autonomous operation eliminates the need for manual intervention, reducing both labor requirements and potential human error while ensuring consistent disinfection coverage. Mathematical modeling confirmed strong linear correlations between exposure parameters and microbial reduction, supporting the optimization of disinfection cycles for maximum efficacy.

In conclusion, the developed UV-C robotic system represents a promising infection control technology that balances high disinfection efficacy with operational safety. Future research should focus on validating the system against a broader range of pathogens, including SARS-CoV-2, optimizing navigation algorithms for dynamic hospital environments, and conducting long-term cost-effectiveness assessments.

4.1. Limitations

The inherent limitation of UV-C technology in treating shadowed areas necessitates integrated disinfection protocols that combine robotic UV-C treatment with conventional chemical disinfection for fully occluded surfaces that receive an insufficient UV-C dose. This represents an important consideration for practical implementation in clinical settings.

4.2. Safety Architecture and Operational Safeguards

The autonomous UV-C robot employs a default-off safety architecture, wherein any sensor malfunction, navigation interruption, or anomaly detection triggers immediate lamp shutdown. Hardware safeguards include automatic deactivation upon collision detection, timer-based operational limits, and remote override capability, complemented by standardized protocols for room clearance verification, warning signage placement, and post-treatment ventilation. This integrated approach aligns with established occupational health frameworks and international guidelines for the deployment of UV-C disinfection in healthcare settings [23, 29, 31].

4.3. Future Development Recommendations

Future developments incorporating Simultaneous Localization and Mapping (SLAM) or LiDAR-based navigation would enhance system adaptability to dynamic clinical environments beyond the structured CT suite configuration. The IR tracking system was selected for this prototype development phase due to lower implementation cost, proven reliability in controlled environments, and ease of maintenance. Future system iterations should incorporate adaptive navigation technologies to enable broader clinical deployment.

5. Declarations

5.1. Author Contributions

Conceptualization, S.E. and K.S.; methodology, B.K., M.T., A.W., T.T., and K.S.; software, B.K., S.P., S.W., and P.A.; validation, B.K., T.T., and K.S.; formal analysis, S.E., M.T., and S.W.; data curation, S.E.; writing—original draft preparation, S.E. and B.K.; writing—review and editing, M.T., A.W., T.T., S.P., P.A., and K.S.; supervision, K.S.; project administration, K.S. All authors have read and agreed to the published version of the manuscript.

5.2. Data Availability Statement

The data presented in this study are available on request from the corresponding author.

5.3. Funding

The authors received no financial support for the research, authorship, and/or publication of this article.

5.4. Acknowledgments

The authors are grateful to the Faculty of Engineering, Faculty of Public Health, Faculty of Allied Health Sciences, and Faculty of Medicine at Burapha University, Chonburi 20131, Thailand.

5.5. Institutional Review Board Statement

Not applicable.

5.6. Informed Consent Statement

Not applicable.

5.7. Declaration of Competing Interest

The authors declare that there are no conflicts of interest concerning the publication of this manuscript. Furthermore, all ethical considerations, including plagiarism, informed consent, misconduct, data fabrication and/or falsification, double publication and/or submission, and redundancies have been completely observed by the authors.

6. References

[1] Mohapatra, R. K., Kandi, V., Gaidhane, A. M., Zahiruddin, Q. S., Rustagi, S., Satapathy, P., Mishra, S., & Tuglo, L. S. (2024). Global domination of the recently VoI-classified 'JN.1' outcompeting other variants - Comparing the vaccines efficacy. Clinical Infection in Practice, 22, 100358. doi:10.1016/j.clinpr.2024.100358.

[2] Hu, B., Guo, H., Zhou, P., & Shi, Z. L. (2021). Characteristics of SARS-CoV-2 and COVID-19. Nature Reviews Microbiology, 19(3), 141–154. doi:10.1038/s41579-020-00459-7.

[3] Peng, M. (2020). Outbreak of COVID-19: An emerging global pandemic threat. Biomedicine and Pharmacotherapy, 129, 110499. doi:10.1016/j.biopha.2020.110499.

[4] Walker, C. M., & Ko, G. (2007). Effect of ultraviolet germicidal irradiation on viral aerosols. Environmental Science and Technology, 41(15), 5460–5465. doi:10.1021/es070056u.

[5] Qureshi, N. S., Villatoro, A. J., Tran, N. D. T., Herrera, S. J., Judge, S. P., Fang, L., Henderson, S. O., & Stanley, K. A. (2024). Hepatitis A Exposure Response and Outbreak Prevention in a Large Urban Jail — Los Angeles County, California, May–July 2023. MMWR. Morbidity and Mortality Weekly Report, 73(6), 131–134. doi:10.15585/mmwr.mm7306a3.

[6] Shen, Y., Liu, Y., Krafft, T., & Wang, Q. (2025). Progress and challenges in infectious disease surveillance and early warning. Medicine Plus, 2(1), 100071. doi:10.1016/j.medp.2025.100071.

[7] Scobie, H. M., Edelstein, M., Nicol, E., Morice, A., Rahimi, N., MacDonald, N. E., Carolina Danovaro-Holliday, M., & Jawad, J. (2020). Improving the quality and use of immunization and surveillance data: Summary report of the Working Group of the Strategic Advisory Group of Experts on Immunization. Vaccine, 38(46), 7183–7197. doi:10.1016/j.vaccine.2020.09.017.

[8] Thongmuang, P., & Suwannahong, K. (2015). Health Behaviours of Undergraduate Students in Suan Sunandha Rajabhat University. Procedia - Social and Behavioral Sciences, 197, 973–976. doi:10.1016/j.sbspro.2015.07.285.

[9] Seeram, E. (2010). Computed tomography: Physical principles and recent technical advances. Journal of Medical Imaging and Radiation Sciences, 41(2), 87–109. doi:10.1016/j.jmir.2010.04.001.

[10] Khalifa, M., & Albadawy, M. (2024). AI in diagnostic imaging: Revolutionising accuracy and efficiency. Computer Methods and Programs in Biomedicine Update, 5, 100146. doi:10.1016/j.cmpbup.2024.100146.

[11] Mossa-Basha, M., Meltzer, C. C., Kim, D. C., Tuite, M. J., Kolli, K. P., & Tan, B. S. (2020). Radiology Department Preparedness for COVID-19: Radiology Scientific Expert Review Panel. Radiology, 296(2), E106–E112. doi:10.1148/radiol.2020200988.

[12] Elias, L. A. A., Nobukuni, M. C., Carvalho, H. E. F. de, Carneiro, L. M., Batista, O. M. A., Sousa, A. F. L. de, Ferreira, A. M., Angeloni, N. L. N., Furlan, M. C. R., Jorgeto, M. F. C., & Junior, A. G. dos S. (2026). Germicidal Ultraviolet C (UV-C) Light for Surface Disinfection in Hospitals: Mapping the Evidence on Devices, Parameters, Effectiveness, and Implementation. Hygiene, 6(1), 14. doi:10.3390/hygiene6010014.

[13] Casini, B., Tuvo, B., Scarpaci, M., Totaro, M., Badalucco, F., Briani, S., Luchini, G., Costa, A. L., & Baggiani, A. (2023). Implementation of an Environmental Cleaning Protocol in Hospital Critical Areas Using a UV-C Disinfection Robot. International Journal of Environmental Research and Public Health, 20(5), 4284. doi:10.3390/ijerph20054284.

[14] van Doremalen, N., Bushmaker, T., Morris, D. H., Holbrook, M. G., Gamble, A., Williamson, B. N., Tamin, A., Harcourt, J. L., Thornburg, N. J., Gerber, S. I., Lloyd-Smith, J. O., de Wit, E., & Munster, V. J. (2020). Aerosol and Surface Stability of SARS-CoV-2 as Compared with SARS-CoV-1. New England Journal of Medicine, 382(16), 1564–1567. doi:10.1056/nejmc2004973.

[15] Mojarad, N., Khalili, Z., & Aalaei, S. (2017). A comparison of the efficacy of mechanical, chemical, and microwave radiation methods in disinfecting complete dentures. Dental Research Journal, 14(2), 131–136. doi:10.4103/1735-3327.205793.

[16] Intensifying vaccine production. (2020). Bulletin of the World Health Organization, 98(5), 302–303. doi:10.2471/BLT.20.020520.

[17] Tessema, B., Gonfa, G., & Hailegiorgis, S. M. (2024). Synthesis of modified silica gel supported silver nanoparticles for the application of drinking water disinfection: A review. Results in Engineering, 22, 102261. doi:10.1016/j.rineng.2024.102261.

[18] Mehta, I., Hsueh, H. Y., Taghipour, S., Li, W., & Saeedi, S. (2023). UV Disinfection Robots: A Review. Robotics and Autonomous Systems, 161, 104332. doi:10.1016/j.robot.2022.104332.

[19] Casini, B., Tuvo, B., Cristina, M. L., Spagnolo, A. M., Totaro, M., Baggiani, A., & Privitera, G. P. (2019). Evaluation of an ultraviolet C (UVC) light-emitting device for disinfection of high touch surfaces in hospital critical areas. International Journal of Environmental Research and Public Health, 16(19), 3572. doi:10.3390/ijerph16193572.

[20] Chotigawin, R., Kandasamy, B., Asa, P., Semangoen, T., Ajawatanawong, P., Phibanchon, S., Pahasup-anan, T., Wongcharee, S., & Suwannahong, K. (2025). Next-Generation Eco-Friendly Hybrid Air Purifier: Ag/TiO2/PLA Biofilm for Enhanced Bioaerosols Removal. International Journal of Molecular Sciences, 26(10), 4584. doi:10.3390/ijms26104584.

[21] Rutala, W. A., & Weber, D. J. (2019). Best practices for disinfection of noncritical environmental surfaces and equipment in health care facilities: A bundle approach. American Journal of Infection Control, 47, A96–A105. doi:10.1016/j.ajic.2019.01.014.

[22] Kowalski, W. J., Bahnfleth, W. P., & Hernandez, M. T. (2009). A Genomic Model for Predicting the Ultraviolet Susceptibility of Viruses. IUVA News, 11(2), 15–28.

[23] Boyce, J. M. (2016). Modern technologies for improving cleaning and disinfection of environmental surfaces in hospitals. Antimicrobial Resistance and Infection Control, 5(1), 10. doi:10.1186/s13756-016-0111-x.

[24] Boyce, J. M., & Donskey, C. J. (2019). Understanding ultraviolet light surface decontamination in hospital rooms: A primer. Infection Control and Hospital Epidemiology, 40(9), 1030–1035. doi:10.1017/ice.2019.161.

[25] Mankar, V., Dhengre, A., Agashe, N., Rodge, H., & Chandi, D. H. (2022). Ultraviolet irradiation doses for coronavirus inactivation -review and analysis of coronavirus photo inactivation studies. International Journal of Health Sciences, 466–472. doi:10.53730/ijhs.v6ns2.5038.

[26] Reed, N. G. (2010). The history of ultraviolet germicidal irradiation for air disinfection. Public Health Reports, 125(1), 15–27. doi:10.1177/003335491012500105.

[27] Różańska, A., Pioskowik, A., Herrles, L., Datta, T., Krzyściak, P., Jachowicz-Matczak, E., Siewierski, T., Walkowicz, M., & Chmielarczyk, A. (2025). Evaluation of the Efficacy of UV-C Radiation in Eliminating *Clostridioides difficile* from Touch Surfaces Under Laboratory Conditions. Microorganisms, 13(5), 986. doi:10.3390/microorganisms13050986.

[28] Resendiz, M., Blanchard, D., & West, G. F. (2023). A systematic review of the germicidal effectiveness of ultraviolet disinfection across high-touch surfaces in the immediate patient environment. Journal of Infection Prevention, 24(4), 166–177. doi:10.1177/17571774231159388.

[29] Anderson, D. J., Chen, L. F., Weber, D. J., Moehring, R. W., Lewis, S. S., Triplett, P. F., Blocker, M., Becherer, P., Schwab, J. C., Knelson, L. P., Lokhnygina, Y., Rutala, W. A., Kanamori, H., Gergen, M. F., & Sexton, D. J. (2017). Enhanced terminal room disinfection and acquisition and infection caused by multidrug-resistant organisms and *Clostridium difficile* (the Benefits of Enhanced Terminal Room Disinfection study): a cluster-randomised, multicentre, crossover study. The Lancet, 389(10071), 805–814. doi:10.1016/S0140-6736(16)31588-4.

[30] Lindblad, M., Tano, E., Lindahl, C., & Huss, F. (2020). Ultraviolet-C decontamination of a hospital room: Amount of UV light needed. Burns, 46(4), 842–849. doi:10.1016/j.burns.2019.10.004.

[31] Cadnum, J. L., Li, D. F., Jones, L. D., Redmond, S. N., Pearlmutter, B., Wilson, B. I. M., & Donskey, C. J. (2020). Evaluation of ultraviolet-c light for rapid decontamination of airport security bins in the era of SARS-COV-2. Pathogens and Immunity, 5(1), 133–142. doi:10.20411/pai.v5i1.373.

[32] Memarzadeh, F., Olmsted, R. N., & Bartley, J. M. (2010). Applications of ultraviolet germicidal irradiation disinfection in health care facilities: Effective adjunct, but not stand-alone technology. American Journal of Infection Control, 38(5 SUPPL.), 13– 24. doi:10.1016/j.ajic.2010.04.208.

[33] Tseng, C. C., & Li, C. S. (2007). Inactivation of viruses on surfaces by ultraviolet germicidal irradiation. Journal of Occupational and Environmental Hygiene, 4(6), 400–405. doi:10.1080/15459620701329012.

[34] Weber, D. J., Rutala, W. A., Anderson, D. J., Chen, L. F., Sickbert-Bennett, E. E., & Boyce, J. M. (2016). Effectiveness of ultraviolet devices and hydrogen peroxide systems for terminal room decontamination: Focus on clinical trials. American Journal of Infection Control, 44(5), e77–e84. doi:10.1016/j.ajic.2015.11.015.

[35] Singh, B. P., Kumar, A., Singh, D., Punia, M., Kumar, K., & Jain, V. K. (2014). An assessment of ozone levels, UV radiation and their occupational health hazard estimation during photocopying operation. Journal of Hazardous Materials, 275, 55–62. doi:10.1016/j.jhazmat.2014.04.049.

[36] Astrid, F., Beata, Z., Van den Nest Miriam, Julia, E., Elisabeth, P., & Magda, D. E. (2021). The use of a UV-C disinfection robot in the routine cleaning process: a field study in an Academic hospital. Antimicrobial Resistance and Infection Control, 10(1), 84. doi:10.1186/s13756-021-00945-4.

[37] Madronich, S., Wagner, M., & Groth, P. (2011). Influence of tropospheric ozone control on exposure to ultraviolet radiation at the surface. Environmental Science and Technology, 45(16), 6919–6923. doi:10.1021/es200701q.

[38] Claus, H. (2021). Ozone Generation by Ultraviolet Lamps†. Photochemistry and Photobiology, 97(3), 471–476. doi:10.1111/php.13391.

[39] Różańska, A., Walkowicz, M., Bulanda, M., Kasperski, T., Synowiec, E., Osuch, P., & Chmielarczyk, A. (2023). Evaluation of the Efficacy of UV-C Radiation in Eliminating Microorganisms of Special Epidemiological Importance from Touch Surfaces under Laboratory Conditions and in the Hospital Environment. Healthcare (Switzerland), 11(23), 3096. doi:10.3390/healthcare11233096.

[40] Palmqvist, C., Samuelsson, A., Fröding, I., & Giske, C. G. (2019). Surface Contamination of CT and MRI Equipment—A Potential Source for Transmission of Hospital-Acquired Infections. Journal of Radiology Nursing, 38(4), 254–260. doi:10.1016/j.jradnu.2019.09.002.

[41] Huslage, K., Rutala, W. A., Sickbert-Bennett, E., & Weber, D. J. (2010). A Quantitative Approach to Defining "High-Touch" Surfaces in Hospitals. Infection Control & Hospital Epidemiology, 31(8), 850–853. doi:10.1086/655016.

[42] Zhou, F., Yu, T., Du, R., Fan, G., Liu, Y., Liu, Z., Xiang, J., Wang, Y., Song, B., Gu, X., Guan, L., Wei, Y., Li, H., Wu, X., Xu, J., Tu, S., Zhang, Y., Chen, H., & Cao, B. (2020). Clinical course and risk factors for mortality of adult inpatients with COVID-19 in Wuhan, China: a retrospective cohort study. The Lancet, 395(10229), 1054–1062. doi:10.1016/S0140-6736(20)30566-3.